APPLIED PHYSICS REVIEWS—FOCUSED REVIEW

Three-dimensional microfabrication of materials by femtosecond lasers for photonics applications

Saulius Juodkazis,[1,2,a)] Vygantas Mizeikis,[3,b)] and Hiroaki Misawa[1,c)]
[1]*Research Institute for Electronic Science, Hokkaido University, N21W10 CRIS Bldg., Sapporo 001-0021, Japan*
[2]*PRESTO, Japan Science and Technology Agency, Kawaguchi 332-0012, Japan*
[3]*Division of Global Research Leaders and Research Institute of Electronics, Shizuoka University, 3-5-1 Johoku, Naka-ku, Hamamatsu 432-8561, Japan*

(Received 9 January 2009; accepted 1 April 2009; published online 11 September 2009)

Femtosecond laser fabrication of three-dimensional structures for photonics applications is reviewed. Fabrication of photonic crystal structures by direct laser writing and holographic recording by multiple beam interference techniques are discussed. The physical mechanisms associated with structure formation and postfabrication are described. The advantages and limitations of various femtosecond laser microfabrication techniques for the preparation of photonic crystals and elements of microelectromechanical and micro-optofluidic systems are discussed. © *2009 American Institute of Physics*. [doi:10.1063/1.3216462]

TABLE OF CONTENTS

I. INTRODUCTION

There is a high demand in modern science and technology for new techniques for micro- and nanostructuring in order to create large structures with small features at high speed. This need, which is primarily driven by the demands of the microelectronics industry, has been fulfilled by the development of a multitude of two-dimensional (2D) lithographic patterning and thin film growth techniques. The performance of these techniques is often characterized using empirical laws, such as Tennant's law,[1]

$$\text{feature size (nm)} = 23 \times \{\text{throughput } (\mu\text{m}^2/\text{h})\}^{1/5},$$

which establishes the relationship between the resolution and throughput of 2D lithography. This law implies that microfabrication of large structures becomes increasingly slow as the size of typical resolution decreases. The use of three-dimensional (3D) fabrication techniques can add new functions to planar 2D devices facilitating miniaturization and make them faster. In recent decades, techniques for 3D structuring of materials have become important tools for the fabrication of photonic crystals (PhCs)[2,3] and other micro-and nanotailored structures with novel photonic functions.[4–6] Methods for high throughput fabrication of structures with small feature sizes are required in order for these new classes of structures to become widespread and practical.

There are three approaches for fabricating 3D PhC structures. The first approach is the a top down approach, in which 3D structures are built in a layer-by-layer fashion using in a succession of steps typically used in traditional 2D lithography and thin film deposition. This approach is usually used for structuring semiconductors with small feature size and has resulted in functional PhC devices.[7,8] However, the throughput of this approach is low because of the very large number of steps required to produce a 3D structure. The second approach is bottom up assembly. This approach includes techniques such as self-organized sedimentation of dielectric nanospheres into ordered 3D opal structures.[9,10] Although this approach allows assembly of very large peri-

[a)]Electronic mail: saulius@es.hokudai.ac.jp.
[b)]Electronic mail: dvmzks@ipc.shizuoka.ac.jp.
[c)]Electronic mail: misawa@es.hokudai.ac.jp.

odic structures with potentially high practical throughput, it provides a very limited choice of 3D periodic lattice symmetry.

The third approach is 3D laser lithography. This methods exploits nonlinear absorption induced by intense laser radiation. This absorption can result in either hard dielectric breakdown in solid dielectrics or "mild" optically triggered cross-linking of polymers in organic photoresists[11–13] and photopolymerizable liquid resins.[14,15] Since the absorption only occurs in areas exposed to high peak intensities of light, and since these areas can be controlled with a high spatial frequency, this method allows for the creation of spatially defined structures in the bulk of transparent materials.

3D laser lithography can be implemented as direct laser writing (DLW) using a focused laser beam,[11,16–18] or by exposure to a periodic optical field created by interference of multiple beams (holographic lithography).[19,20] 3D laser lithography can be thought of as 3D "photography" and it includes both top-bottom approaches (e.g., drawing by the laser beam in direct writing) and bottom-top approaches (e.g., "self-organization" of the interference pattern of multiple beams). By using femtosecond laser pulses with high peak fluences, it is possible to achieve nonlinear two-photon absorption (TPA) or multiphoton absorption (MPA) in a wide range of materials at low average incident powers. Hence this technique could potentially provide a cheap and accurate method for high throughput fabrication of photonic structures. DLW can be implemented in conjunction with other techniques such as exposure to intense surface plasmon optical near field[21] or by combining it with various postprocessing techniques, such nanoimprinting[22] and infiltration by other materials[23] (a recent review can be found in Ref. 24), thereby increasing its versatility. Laser lithography also provides ample scope for optimizing the optical exposure regime to yield the desired structure. This can be done by proper selection of the photosensitive materials and by controlling the exposure wavelengths and the laser pulse durations. DLW has already been used to deliver high-resolution periodic 3D PhC structures of good structural quality.[25–27] The low refractive index contrast and consequent lack of 3D photonic band gap (PBG) can be corrected without loss of structural quality by infiltrating the optically fabricated *templates* with high refractive index materials, such as silicon. Polymeric 3D templates can also be infiltrated by metals (e.g., silver), thereby converting the structures into 3D metamaterials.[28]

These days, when the economical and environmental impacts of new technologies are subject to extensive scrutiny, laser lithography emerges as a favorable technology for 3D microfabrication. This is because (a) commercial ultrafast lasers, which are the most expensive equipment required for laser lithography are widely available and becoming less expensive. (b) It involves minimal chemical postprocessing, and (c) it does not require expensive and energy consuming high-vacuum or ultraclean environments. Also, use of materials to make a 3D microdevice is small and can be produced with less waist, which are economically and environmentally desired features.

Thus, 3D nanostructuring of materials by femtosecond laser pulses is likely to become the leading technology for fabricating new classes of 3D micro-and nanostructures in the foreseeable future. The aim of this paper is to provide an overview of 3D laser lithography, and its application for the fabrication of 3D PhC structures. The structure of the paper is as follows. Section II provides an overview of the applications of 3D structured materials. Section IIIdiscusses the experimental aspects of laser lithography and the various postprocessing steps. Finally, the structural and optical characteristics of structures obtained by optical lithography are described in Section IV.

II. 3D STRUCTURED MATERIALS: OVERVIEW OF FABRICATION AND APPLICATIONS

In this section we will outline the application fields of PhC structures. The general properties of PhCs, their structural and optical properties, the role of dimensionality, and routes to their fabrication are beyond the scope of this paper. These details can be found in the available excellent textbooks.[29,30] It is worthwhile noting that in addition to artificial PhC structures, there are a number of naturally occurring periodically structured dielectric materials that exhibit the basic functionality of PhCs. Gemstone opal is the best-known representative of this class. The wings of some butterflies are also known to exhibit distinct colors that are controlled via optical scattering caused by submicrometer-scale periodic structures on the wing, rather than by pigments and absorption.[31] These naturally occurring phenomena suggest a potential application for PhC structures in the production of environmentally friendly, pigmentless dyes, and significant efforts are being made to reproduce these effects with artificial structures.[32] In the future, laser lithography may be applied for rapid fabrication of structures that mimic naturally occurring PhC systems.

Electrochemical anodization of metals and semiconductors can also be used to form complex 3D patterns. For instance, anodic alumina can be formed from metallic Al.[33] Similarly, ordered nanomicroporous silica-silicon composites can be made out of crystalline Si.[34] A pattern is formed on the surface of the sample by a lithographic or embossing technique[35] creating pits from where electrochemical structuring is guided. Due to the high refractive indices of alumina and silicon and since the period of the structure can be defined with a high submicrometer resolution, these 2D structures can be used for PhC applications.[36] The anodic etching of silicon can be used to create nanocrystals of Si which are encapsulated in the complex network of a nanoporous silica host and are efficient emitters of blue photoluminescence. Various chemical and physical control methods, such as the use of auxiliary illumination, can be applied to guide 3D structuring of silicon.[37–41] An extension of such methods is the light-induced back side wet etching which can be applied to structure dielectric materials.[42–44] In this technique, light is used as an electron-hole excitation source which is made by projecting an optical image of the pattern through the sample (transparent at the used wavelength) onto the back side boundary with an etchant solution. High-aspect ratio (>100) structures can be formed by wet etching medi-

ated via complex thermal and cavitation effects for micro-optical and fluidic applications. This technique can yield structures with micrometer resolution.

Liquid crystals are active materials in which large refractive index changes can be induced either by thermal or optical means. Light-crystal displays are examples of how 2D structures of liquid crystals can be used for fast optical modulation of transmission. An extension of this planar 2D technology into a 3D realm is highly anticipated and is expected to open new applications in adaptive optics and lead to the development lenses with changable focal lengths for visual aides and goggles. It is also expected that these types of structures will be integrated into microfluidic, optofluidic,[45,46] and microelectro mechanical system/micro-optomechanical system (MEMS/MOEMS) devices.[47] Cholesteric liquid crystals are a class of chiral materials that could be used to create PhCs with photonic stopband (PSB) and polarization stopband in the UV-to-IR range.[48] The pitch of the chiral structure can be controlled by thermal quenching of the cholesteric liquid crystal[49] or via the concentration of the chiral agent which is mixed with a nematic phase liquid crystal. They could be used for creating a variety of microphotonic devices such as microlasers.[50–53] PhCs with stop gaps from the visible to IR spectral ranges are readily obtainable, and recently, laser lithography was successfully used to fabricate PhCs with chiral architectures bearing resemblance to those of liquid crystals.[18,54–56]

One of the requirements for obtaining a functional PhCs is a substantial refractive index contrast within the structure. Even the most favorable geometries for the opening of full PBG need at least a 1 : 2 index ratio. Most of the available photoresists and resins have refractive indices $n < 1.7$ at optical wavelengths, and consequently, PhCs fabricated in these materials can only exhibit PSBs but not PBGs. Nevertheless, the index contrast can be enhanced by infiltrating materials with high refractive indices such as silicon into the initial polymeric structures. Optically fabricated PhCs are therefore often regarded as templates intended for further enhancement.

III. EXPERIMENTAL METHODS FOR 3D STRUCTURING

In this section, we will describe two methods for laser fabrication of 3D PhC structures: (a) direct laser (DLW) and (b) holographic recording by multiple beam interference.

A. Direct laser writing

Practical methods for implementing DLW have been widely described in the literature for surface and in-bulk structuring of materials.[11,57–62] These methods differ from one another in details, such as the laser wavelength, pulse duration, and repetition rate, or the method of beam translation inside the sample. However, the general experimental setup is essentially the same in all cases and is illustrated in Fig. 1. A femtosecond laser beam is tightly focused into the bulk of the sample, which usually comprises a thin film of photoresist or another material deposited on a supporting glass substrate. The laser light is absorbed via nonlinear TPA or MPA processes at the focus, leading to a photoresponse

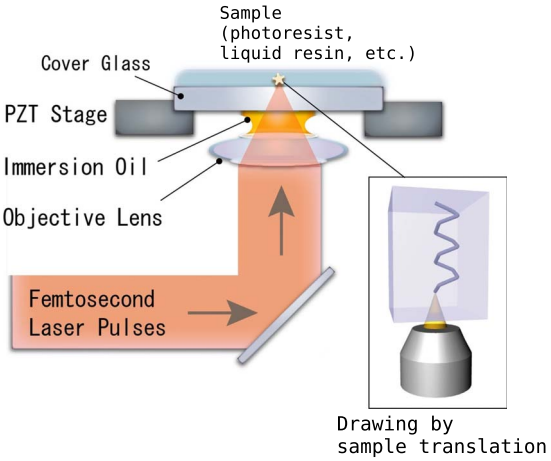

FIG. 1. (Color online) Optical setup for laser lithography by DLW. The inset illustrates drawing by translation of the focused laser beam inside the sample.

such as photopolymerization or optical damage, within the absorbing material. It is noteworthy that depending on materials and irradiation conditions, the nonlinear absorption is acting as a seeding excitation for more efficient avalanche excitation followed by recombination and heating which become more efficient material modifiers. 3D features are then drawn by translating the focal spot inside the sample. This translation could be accomplished using high-accuracy translation stages, controlled, for example, by piezoelectric transducers (PZTs). Alternatively, the laser beam could be translated inside the sample using mirror deflectors. It is noteworthy that spatially and temporarily shaped laser beams, e.g., Gauss–Bessel beams/pulses, can be used for recording axially long patterns.[63] Similarly, the phenomenon of filamentation can be applied to create axial intensity distributions which are useful for applications.[64]

Nonlinear absorption is essential for DLW, since it provides conditions whereby the converging laser beam can propagate into the material without experiencing significant losses until it reaches an intensity concentration that is sufficient to induce the modification initiating TPA/MPA in the focal plane of the lens. The use of nonlinear mechanism also ensures that the spatial profile of the nonlinear exposure is steeper than the optical intensity profile. Since the photoresponse of the exposed materials typically has an intensity threshold (e.g., a threshold for inducing photopolymerization or optical damage), one can induce photomodification in an area smaller than the diffraction-limited focal spot size by carefully adjusting the laser intensity. If a high numerical aperture (NA) lens is used for focusing, the photomodification can be localized to within subwavelength sized regions at the focal spot, leading to structures that can be defined with subwavelength resolution reaching feature sizes of tens-of-molecular cross sections. This resolution of 3D structuring is approaching that of focused ion beams (FIBs).[65]

In our optical lithography experiments, we use a femtosecond Hurricane X system (Spectra-Physics) with a temporal pulse width $\tau_{pulse} = 130$ fs and a central wavelength $\lambda_{laser} = 800$ nm. The laser beam is focused by an oil-immersion lens with NA=1.4, which produces a spot with a diameter at

waist of $d_0=0.61\lambda/\mathrm{NA}\simeq 0.7\ \mu$m (at e^{-2} intensity level) in the focal plane. The sample is translated using a 3D PZT-controlled stage, whose trajectory of motion is defined and controlled using a personal computer.

The type of photomodification that occurs within the focal spot depends on the material used and the optical exposure regime. Optical damage in solid materials usually requires powerful laser radiation. However, it can easily be achieved even at low average laser powers if femtosecond pulses are used.[66] Femtosecond laser induced optical damage completely or partially obliterates the material, creating voids surrounded by densified shells.[67–70] Creating this kind of photomodification is straightforward. However, the explosive nature of the process often results in extensive structural defects such as cracking. At intensities below the optical damage threshold, refractive index modification by an amount of about $\sim 10^{-3}$ can be induced without structural damage. However, functional PhCs require a high refractive index contrast. Hence this regime of exposure is not suitable for their fabrication and is better suited for recording structures such as channel-type optical waveguides[71] which do not require a high refractive index contrast. In some cases it is possible to enhance the performance of periodic channel structures recorded with strong or partial damage by removing the optically affected material using wet chemical etching.[72]

Another type of optical photomodification that is widely used for optical fabrication of PhCs is photopolymerization of liquid resins[73,74] or organic photoresists.[75] Photopolymerization can be initiated via TPA/MPA by tightly focused femtosecond pulses at nanojoule pulse energies followed by chemical and thermal processes of polymerization. This kind of photomodification is initially latent and only becomes visible after the unexposed material is removed (in liquid resins by washing, and in solid photoresists by chemical development). The fact that postprocessing is required in order to reveal the recorded structures is favorable for PhC recording. This is because the recorded features do not obstruct optical access to deeper regions of the material and do not limit the freedom of the laser drawing process. In this paper we will mainly describe applications of DLW in a commercial epoxy-based negative photoresist, SU-8 (Micro Chem).[76] This photoresist is photosensitive in the linear regime at wavelengths below 360–400 nm and is therefore highly suitable for TPA/MPA excitation at the laser wavelength of 800 nm. Furthermore, it has a high spatial resolution and was specifically designed for optical fabrication of high aspect ratio structures intended for use as elements of micromechanical systems. Hence, extended 3D structures can be fabricated by DLW in thick films of SU-8. The largest shortcoming of SU-8 is that it exhibits shrinkage, which is reported to be about 7% (which is strongly dependent of thickness and area size of the structure). This shrinkage can lead to deformation of the recorded structures. However, various modifications in pre- and postfabrication processing of the samples can help to alleviate this shortcoming.

B. Holographic recording

Holographic recording is another approach widely used for optical fabrication of periodic PhCs.[77] It is based on exposing a photosensitive medium to a periodic interference field created by several coherent laser beams that overlap at nonzero mutual angles.[78,79] In general, the interference field intensity distribution $I(\mathbf{r})$ can be expressed as a superposition of coherent plane waves,

$$I(\mathbf{r}) = \sum_{n,m} \mathbf{E_n} e^{-i(\mathbf{k_n}\cdot\mathbf{r}+\delta_n)} \cdot \mathbf{E_m^*} e^{i(\mathbf{k_m}\cdot\mathbf{r}+\delta_m)}, \quad (1)$$

where $\mathbf{E}$ is the complex electric field vector, $\mathbf{r}$ is the radius vector, $\mathbf{k}$ is the wave vector, and $n=m$ represents the number of interfering beams. The phases of the beams are given by $\delta_{n,m}$.

Multiple coherent beams can be conveniently obtained from a single beam using a special diffractive optical beam splitter or diffractive optical element (DOE).[19,80] The original beam passes through the element and is split into a number of divergent beams through diffraction. These beams propagate at nonzero angles with respect to the zero-order transmitted beam. The beams are then collimated by a lens, and a mask is used to select the beams required to form the desired interference pattern. The symmetry of the interference pattern can be optimized by controlling the beams, amplitudes, phases, and polarization by waveplates, phase retarders, and filters.[80,81] The selected beams are then redirected with a second weak lens so that they converge on the photosensitive sample. Depending on the NA of the focusing lens, it can create mutual angles of up to 60°–80° between the beams. The most attractive feature of using DOEs for creating PhCs is the fact that when the incident beam is pulsed, the emerging beams have tilted intensity fronts parallel to that of the initial beam, despite their different propagation directions. Overlapping such pulses on the sample by focusing automatically ensures spatiotemporal coincidence in the entire region of their interference without need for additional adjustment.[82] Hence, interference patterns can be recorded in areas with cross sections approaching 1 mm[19,20,83] even when the intensity envelope of the pulses has a length of about 30 μm. For comparison, pulses produced by an ordinary beamsplitter would only overlap in a cross-sectional area of $c\tau_p/\sin(\theta)$, where c is the speed of light, τ_p is the pulse duration, and θ is the half-angle between the pulse propagation directions.[84]

The fundamental limitation of a simple optical setup based on a DOE is that the maximum achievable angle between the beams is limited to about ~80°. Larger angles could be obtained by using high NA lenses to redirect the beams. However, this would limit the size of the irradiated area and result in more oblique incidence angles which might lead to unwanted back and internal total reflection of the incident beams at the sample. On the other hand, the period of the interference pattern depends on the angle between the interfering waves, and fabrication of patterns with periods comparable to the recording wavelength requires one to increase the angles of overlap/incidence. More important is the fact that in order for the PhC to exhibit direction-independent

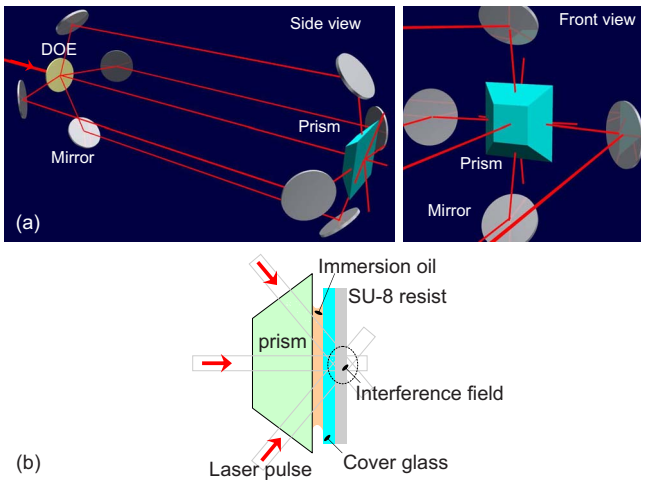

FIG. 2. (Color online) (a) Schematic explanation of optical lithography by multiple beam interference for the case of five beams produced by a DOE. For simplicity, optical delay lines necessary in order to achieve temporal coincidence of short laser pulses are not shown. (b) Sample mounting geometry.

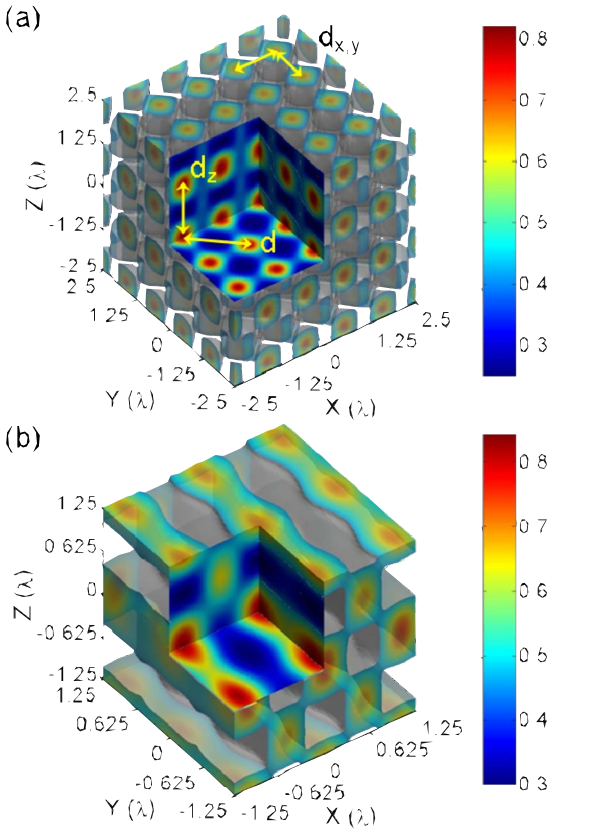

FIG. 3. (Color online) Theoretically calculated light interference pattern formed by five beams overlapped using the setup shown in Fig. 2. (a) for scalar superposition (i.e., fields are added as $[(1+1+1+1)(\text{peripheral})+4(\text{central})]^2$ and then squared), (b) for vectorial superposition that takes into account linear polarization of the initial beam along the y-axis direction (i.e., fields are added as $\{[1x+1x+\cos(70.53°)y+\cos(70.53°)y]\times(\text{peripheral})+4(\text{central})\}^2$ with factor cos(70.53°) representing projection of the **E**-field on y-axis). Coordinates x, y, and z are normalized to the laser wavelength.

PBGs, the crystalline unit cell of these structures should satisfy certain symmetries. These requirements on symmetry are typically fulfilled by cubic cells, which have equal lengths along all three spatial coordinates. It can be demonstrated that oblique incidence angles of the beams are required in order to obtain this symmetry. This has prompted various groups to abandon the convenience of DOEs in favor of traditional reflective beamsplitters for PhC fabrication when the equal lateral and axial periods must be obtained. This then requires them to use separate elements for adjusting the amplitude and phase for each of the participating beams. However, even with this setup tricks for suppressing the total internal reflection are still required. One approach for doing this is to use a special prism to overlap the beams at high angles to the sample surface normal[85] as illustrated in Fig. 2. This setup enables alignment of the five beams (including the central transmitted beam) required for the interference field that can produce structures with a cubic unit cell. In this setup, the angle of incidence of side beams with respect to the oriented facets of the prism is low, and thus eliminates the total internal reflection.

It has been demonstrated that in order to form a cubic unit cell, the angles of incidence of the four side beams must be $\theta=70.53°$, and that controlling the polarization of all five beams allows for the creation of an interference pattern with a diamond structure. This possibility is especially interesting, since the diamond structure is widely recognized as the most favorable structure for creating spectrally wide and spectrally robust 3D PBG, provided that the refractive index contrast is sufficiently large ($\Delta n > 2$) considering a silicon as the candidate material for applications merging of photonic and electronic circuitry on a microchip.[86] Figure 3 shows examples of the five-beam interference intensity distribution calculated according to Eq. (1). The set of beams is assumed to consist of a central beam whose axis of propagation coincides with the main optical axis of the system (parallel to the z-axis) and four peripheral beams with angles of incidence of $\theta=70.53°$ with respect to the central beam. The directions of propagation of these beams can be described in terms of their wave-vector components in the x-y plane (k_x,k_y) as $(k_0,0)$, $(0,k_0)$, $(-k_0,0)$, and $(-k_0,-k_0)$, where $k_0=(2\pi/\lambda)\cos(\theta)$. The polarization of the beams is linear and parallel to either the x or y axis. The calculated interference patterns exhibit a cubic unit cell whose symmetry can be described as face-centered cubic (fcc). The fcc structure is expected for an ideal interference pattern created by beams with identical linear polarization parallel to the sample plane [this would correspond to $\cos(\mathbf{E}_n\hat{\mathbf{E}}_m)\simeq 1$ for all pairs of (n,m) beams]. In fact, all beams have different transverse and longitudinal polarization components with respect to the sample plane at large angles of incidence. Figure 3 demonstrates the ideal (a) and actual (b) interference patterns. In the latter case, for the y-polarized side beams (only the $\mathbf{E}_y$ component is present), the intensity modulation along the x-axis differs from the intensity modulation along the y-axis. Consequently the structure is more channel-like than the expected fcc as shown in panel (b). A practical solution for this problem is to increase the intensities of the two side pulses to create a weaker intensity modulation.

Figure 3 also illustrates that if the parameters of the interference beam are chosen appropriately, then the fcc unit cell acquires a two-"atom" basis and is transformed into a

diamond structure. Closer analysis of the pattern reveals that the lattice period of the five-beam interference field d in the x-y plane is related to the distance between "atomic" planes d_{xy} (see Fig. 2) as $d=\sqrt{2}d_{xy}$, where $d_{xy}=\lambda/\sin(\theta)$, while the distance between planes along the z-axis is $d_z=\lambda/[1-\cos(\theta)]$; hence, $d=1.5\lambda$, where λ is wavelength in the material. Thus, for fixed directions of incidence, the lattice period can be tuned most easily by tuning the laser wavelength. Further examples of various patterns obtainable by holographic recording technique will be given in Sect. IV B.

From a technical point of view, the prism-based setup is easy to implement with continuous wave or pulsed nanosecond lasers, but its realization becomes a challenging task when it is intended for use with femtosecond pulses. Short-pulse excitation is indispensable for nonlinear photoexcitation (high intensity/irradiance is obtained even for small pulse energy), and therefore methods for simplifying the procedure for forming the interference pattern formation, while simultaneously maintaining the spatiotemporal overlap and high incidence angles of the beams are actively being pursued. These efforts have led to designs in which a diffractive element is used for beam splitting, and the interference region is located next to the splitter, where a film of photosensitive medium is attached. One of the recent proposals uses a stack of two gratings with grooves oriented at a 90° angle, separated by a thin spacer layer to produce the five interfering beams needed for the formation of a 3D diamond structure.[87] A similar, but simpler design using gratings of different heights was also recently demonstrated.[88] In these designs selective generation of only five beams is achieved by making sure that the lattice periods are to sufficiently short, thereby making the higher diffractive orders nonpropagating. Thus only the central zero-order beam and four diffracted beams emerge to form the required set. Alternatively, the required 3D intensity distribution can be created by irradiating a mask comprising a 2D array of nanoholes made in aluminum.[89] This method falls into another category of surface-plasmon-assisted techniques and allows fabrication of high-resolution structures with a period of ~400 nm. The mask-based designs are still being developed, but they could potentially offer simple and cost-effective methods for preparing 3D PhCs.

IV. RESULTS AND DISCUSSION

A. Direct laser writing

Direct laser writing has been used to fabricate a variety of microstructures including optical waveguides,[90] PhCs,[14,91,92] void channels and microfluidic devices,[93,94] as well as for 3D optical data storage in various glasses[95–99] and polymers[100] by use of femtosecond pulses.

In addition to the simple implementation of DLW described in Sec. III, more complex experimental realizations are possible in which DLW is performed by multiple beams simultaneously. The multiple beams are focused/formed using multiples arrays[101,102] or Fresnel lenses. In principle, the optical function of a single lens or array of lenses with dynamically adjustable parameters can be created using a spatial light modulator (SLM), which can spatially modify the phase of the laser pulses and modify the pulse front in order to minimize spherical aberrations at the focus.[103] The spherical aberration has usually the largest contribution for the focal volume distortions, which depend on the refractive indices of sample and its ambient as well as on the depth of the focal position. The advantage of beam shaping based purely on phase modulation is its lossless nature. The use of a SLM can be combined with a system for scanning the sample's position to increase the versatility of the DLW system,[104] and to provide dynamic compensation for distortions and aberrations to the beam.

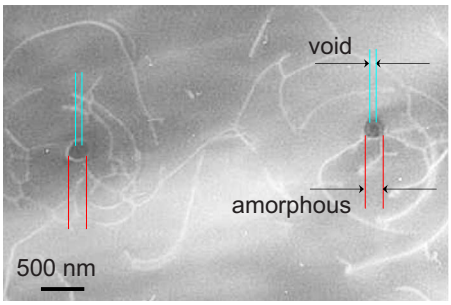

FIG. 4. (Color online) TEM image of voids in sapphire separated from each other by a distance of 3.5 μm. The image plane corresponds to c-plane of sapphire (001). The recording was done by 80 nJ energy pulses at a 20 μm depth from the surface. The NA of the focusing objective lens was NA =1.35.

1. DLW via optical damage

Optical microstructuring with subwavelength resolution, especially via optical damage, is generally easier using high peak power laser pulses. By tightly focusing femtosecond pulses it is possible to minimize thermal or other nonoptical effects, thereby enabling larger volumetric density of controlled modification within a given region. Pulses with energies of hundreds of nanojoules typically record voids surrounded by shells of densified material that form due to the action of shock-wave pressure that follows the optical damage.[67,105,106] The pulse energy needed to form voids was found to be lowest in glasses with high concentrations of glass-forming oxides, and in crystals where atomic bonding is efficiently re-established after the dielectric breakdown.[67,68,107,108]

Optical recording via dielectric breakdown in crystalline materials and glasses creates voids with the largest possible contrast of refractive index and mass density very fast within few nanoseconds.[106,109] The recorded structures can be used for applications such as optical data storage, and the creation of waveguides, and PhCs. Unfortunately, fabrication by damage can also lead to significant structural irregularities. Figure 4 shows a transmission electron microscopy (TEM) image of two isolated voids recorded in sapphire. For the observation, two-sided polishing of the sample was performed. The images show that the voids have diameters of less than 100 nm and are surrounded by material that has been subjected to significant stress, resulting in a number of dislocations. These regions extend to a distance of about 1–2 μm away from the void. In structures comprising large numbers of closely packed voids the stress will relax by in-

curring extensive structural damage, such as macroscopic dislocations and cracks. This damage will degrade the mechanical properties and stability of the structures.[67,110]

The character of the optically induced modification (via damage or other mechanisms) that occurs at the focal point depends strongly on the light intensity distribution of the focused beam. The intensity distribution for a focused ideal Gaussian beam is well known; however, real beams, especially those delivering pulses of subpicosecond duration, may differ significantly because of various distortions and imperfections, both in the initial beam and in the focusing optics. Consequently, the actual irradiance at the focus may be somewhat lower than expected. Spherical aberrations are the main distortions in high refractive index ($n \sim 2.0$) materials and/or at large focusing depths. >50 μm.[111–114] Chromatic aberrations also become significant for pulses shorter than 100 fs. Tilt of the pulse front (the spatial chirp) may also limit the sharpness of focusing.[109,115] Second order dispersion in high NA oil or water-immersion objective lenses can result in pulse chirpt of up to 5000 $1/\mathrm{fs}^2$.[116] Axial misalignments of the beam are also common, but they can be eliminated by proper alignment of the optical setup. It was recently demonstrated that the pulse front can be reliably controlled using a SLM composed of a liquid-crystal matrix. Using this device the intensity distribution at the focus can be made nearly aberration-free.[103]

Optical recording via dielectric breakdown can also be used to form voids in softer organic materials,[69,117,118] either as isolated damage spots or channels obtained by smooth translation of the focal spot. This approach was applied for the fabrication of PhCs.[59,70,119]

2. The effect of optical field enhancement on the optical breakdown

Ultrashort, tightly focused laser pulses may easily induce nonlinear absorption in transparent materials and create strong ionization even at intensities below the dielectric breakdown threshold. Electron-hole (e-h) plasma formation in an intrinsically dielectric material will modify its dielectric constant ε, causing the real part of the constant to approach zero value at complete ionization at plasma frequency. Interactions between the incident optical field and the dynamically modified plasma regions can lead to optical damage with characteristic localization patterns. For instance, multipulse excitation can result in ripple damage in glasses and crystalline materials.[120] Theoretical analysis has indicated that photogenerated point defects play a crucial role in this process. Initially the defects are created at the locations of photoionization at the lowest incident fluences; the defects are stochastically distributed. They then accumulate under multiple-pulse exposure. The defect sites are initially just plasma seeds, but they are subsequently transformed into rapidly expanding spherical plasma regions as a result of multiphoton and impact (avalanche) ionization. During the seeding stage, the initial plasma breakdown regions are of nanometric size, and their evolution is governed by the local field. The small, subwavelength size of the plasma seed regions validates the use of the electrostatic approach for deducing the local field,[120]

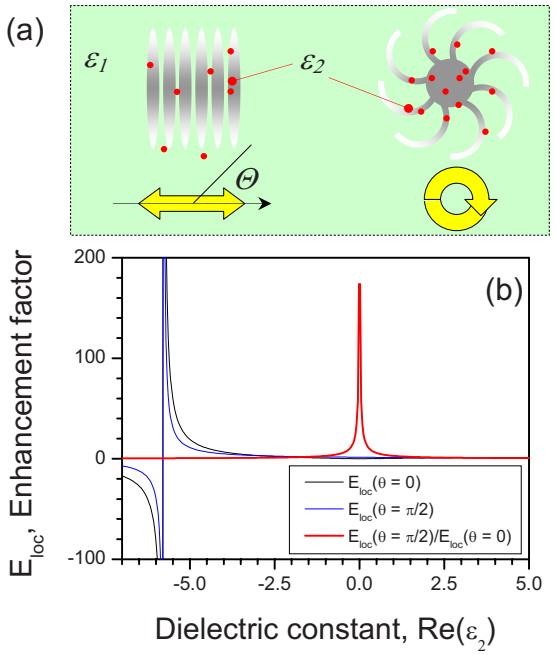

FIG. 5. (Color online) (a) A Schematic representation of the optical field enhancement spatial patterns (the gray regions mark structural changes) formed inside a dielectric due to e-h plasma generation at the defect sites (denoted by the dots) for linear and circular polarized excitation. (b) Dependence of the local field E_{loc} calculated according to Eq. (2) for a sapphirelike material with $\varepsilon_1 = 1.7^2 = 2.89$ assuming the incident field of $E=1$ and its enhancement factor $E_{\mathrm{loc}}(\varepsilon_2, \theta = \pi/2)/E_{\mathrm{loc}}(\varepsilon_2, \theta = 0)$ vs the real part of dielectric constant in the breakdown region.

$$\mathbf{E_{loc}} = \frac{3\sqrt{\varepsilon_2^2 - (\varepsilon_2^2 - \varepsilon_1^2)\cos^2(\theta)}}{\varepsilon_1 + 2\varepsilon_2}\mathbf{E}, \tag{2}$$

where $\varepsilon_{1,2}$ is the real part of dielectric constant in the intact and damaged regions, respectively, θ is the angle between the polarization direction and orientation of the plasma region, and $\mathbf{E}$ is the electrical field vector of the incident radiation.

Figure 5(b) shows the local field as a function of the real part of the dielectric function at the dielectric breakdown (nanoplasma) sites when calculated according to the above equation. It illustrates that field amplitude enhancement by factors of $10^2 - 10^3$ are achievable for $\theta = \pi/2$. Due to the angular inhomogeneity of the enhancement, plasma spheres evolve into plasma nanosheets, leading to the formation of planar damage structures in the case of linear incident polarization, and chiral structures in the case of incident circular polarization, as illustrated schematically in Fig. 5(a). Somewhat stronger local field enhancements are expected when nanoparticles of gold, silver, or copper are incorporated into the dielectric.[121,122] This suggests that efficient formation of ripple structures could occur in glasses containing suspensions of noble metals.

3. Direct laser writing via photopolymerization

DLW by photopolymerization triggered by nonlinear absorption at the focus of a femtosecond laser beam is a mechanism that has been widely used for the fabrication of a

wide variety of micro- and nanostructures. There are two types of materials that are frequently used for such DLW: liquid resins and solid photoresists.

In liquid resins, optical exposure leads to an almost instantaneous liquid to solid phase transition. The DLW process is most "direct," and the only postprocessing procedure needed is removal of the unexposed liquid by washing in a proper solvent. There are several kinds of liquid resins that are commercially available. For example, urethane acrylate resin (SCR500; JSR, Japan) with added photoinitiators sensitive in the blue or ultraviolet spectral ranges are suitable for two-photon fabrication using lasers operating at visible and infrared wavelengths. Other popular liquid resin photopolymers are Nopcocure 800 (San Nopco, Japan) and the Norland (Norland Products, Inc.) optical adhesive NOA series (e.g., NOA63, NOA68). Resins have a high spatial resolution, but they also exhibit significant shrinkage after the fabrication which may lead to deformation of the fabricated microstructures.

Unlike resins, photoresists are initially solid, and their photomodification (via polymer cross-linking or other mechanisms) after the optical exposure is latent. Wet chemical development is usually required to complete the fabrication process. The solid photoresists that is most commonly used for DLW (and also for holographic recording) is SU-8. SU-8 was designed for optical fabrication of micromechanical and microfluidic parts with high aspect ratios. SU-8 contains a photoinitiator, triphenylsulfonium hexafluoroantimonium, which also acts as a photoacid generator (PAG) that enhances the propogation of the polymerization process. It absorbs at the excimer laser wavelength of 308 nm. Direct measurement of the fluorescence excitation spectrum of SU-8 shows that it has an absorption band around 310 nm. A PAG with a similar structure, Ignacure OXE01, has a maximum TPA cross section of 30 GM at a wavelength of 660 nm and an absorption cross section of only 2 GM at 800 nm.[123] Exposure to UV radiation (in the linear regime) or to high-irradiance IR radiation (in the nonlinear regime) causes the PAG-amplified cross-linking of molecular chains of SU-8. Solidified SU-8 becomes material resistant to the subsequent development.

The mechanisms of nonlinear photopolymerization of SU-8 and other resists by IR femtosecond pulses are not yet fully understood. The nonlinear polymerization of SU-8 shows a weak dependence on wavelength in the 780–1100 nm range. Also, the typical pulse irradiance of $\sim 1\ \mathrm{TW/cm^2}$ used in photopolymerization is close to the dielectric breakdown of polymers.[117] Hence, the exposure and polymerization take place within a strongly ionized medium and the chemical pathways of typical PAG-enhanced polymerization are expected to be strongly altered. Radiative and thermal exposure of photopolymers during thermal equilibration of hot electrons with emission at the strong molecular absorption window of polymers at $2-3\ \mu\mathrm{m}$ can explain the polymerization of SU-8.[124] This mechanism is also expected to be relevant for other types of polymerization processes such as cationic, anionic, or free-radical polymerization. In addition to organic photoresists, hybrid organic-inorganic materials synthesized via sol-gel processes, such as commercial ORMOCER (Ref. 125) and zirconia-silica composites with methacrylate SZ2080 (Ref. 126) are becoming increasingly popular due to easy preparation and development and due to possibility to fabricate 3D structures of high spatial resolution. It has been demonstrated that the higher laser power causes sol-gel resist to shrink[127] and this improves resolution, which is usually not the case in other discussed photopolymers. It is helpful to note that the organic-inorganic resists are biocompatible, which means that the recorded structures could possibly be used as scaffolds for cell culture. Also, annealing can be used to ash the organic part when required.

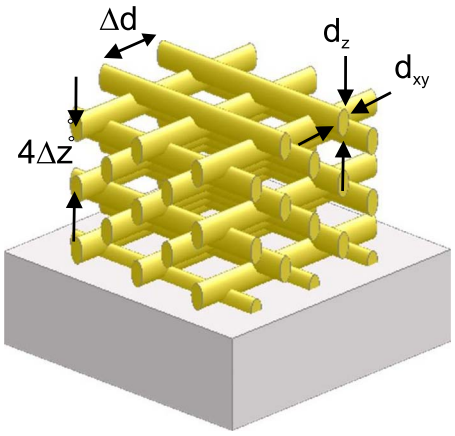

FIG. 6. (Color online) Woodpile structure composed of layers of dielectric rods separated by the distance Δd and Δz in the x-y plane and along the z-axis, respectively. The rods have ellipsoidal cross sections with minor and major diameters d_{xy} and d_z respectively. The elongation of the ellipse along the z-axis direction is coincident with the focusing direction of the propagating laser beam. The structures are usually fabricated while the template is attached to glass substrate.

The DLW process provides unprecedented flexibility in the choice of structure topology, which is only limited by the requirement that the final structure should be mechanically stable and withstand postprocessing (development, infiltration). This technique has been successfully applied for the fabrication of PhC templates with woodpile, square and circular spiral, chiral, and slanted-pore topologies.[11–13,15,17,18,54,128,129]

PhCs with the so-called woodpile architecture are examples of structures that can be recorded by DLW via photopolymerization.[130] A schematic description of the woodpile structure and its main parameters are given in Fig. 6.

Figures 7(a)–7(c) show scanning electron microscopy (SEM) images of a woodpile structure fabricated by DLW in SU-8. The woodpile structure was drawn by smooth translation of a laser beam with a velocity of $50\ \mu\mathrm{m/s}$, which ensured that the distance between the centers of two neighboring exposed spots was 50 nm. The woodpile is supported by massive SU-8 walls because structures having lateral dimensions in excess of $50\ \mu\mathrm{m}$, and lateral diameters of the rods less that approximately 300 nm are easily distorted by SU-8 shrinkage (up to 7%) and by the action of capillary forces during postdevelopment drying. The walls, together with special steps aimed at minimizing the capillary forces (see Sec. IV C 1), help to obtain woodpile structures with suffi-

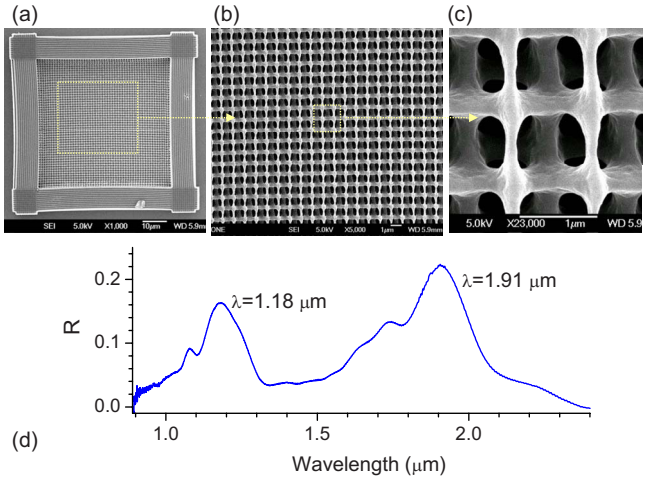

FIG. 7. (Color online) [(a)–(c)] SEM images of a woodpile structure fabricated by DLW in SU-8. The structure parameters are $\Delta d=1.0\ \mu$m, $\Delta z=0.55\ \mu$m, size of $60\times60\times12\ \mu$m^3, the number of woodpile layers is $m=22$. During the fabrication the focusing oil-immersion lens used had 60× magnification and a numerical aperture of NA=1.4. The laser pulse energy was 0.4 nJ. The central wavelength was 800 nm, and the pulse duration was 150 fs. (d) The measured optical reflectivity spectrum of the woodpile structure.

cient quality for the observation of PSGs. As illustrated by Fig. 7(d), the fabricated woodpile exhibits reflective bands near the 1.91 and 1.18 μm wavelengths due to the PSG along the woodpile layer stacking direction coincident with the z-axis. As shown, the resolution of the DLW is sufficient for obtaining polymeric structures with PSGs at near-infrared and telecommunications spectral wavelengths. Other examples of 3D PhCs fabricated in SU-8 can be found in the literature.[11–13,15,17,18,54,128,129]

The flexibility of the DLW technique can be exploited not only for fabrication of periodic PhCs but also for fabrication of elements for MEMS and MOEMS systems. Waveguides, channels, springs, and cantilevers can easily be fabricated using this approach and integrated into fluidic and MEMS/MOEMS devices. One can also exploit the elastic properties of cross-linked polymers. For example, the resonant frequency of a 50 μm long cantilever with a radius of 1 μm consisting of fully cross-linked SU-8 (with Young modulus $E=4$ GPa) is[131]

$$f_0 = \frac{3.516}{2\pi l^2}\sqrt{\frac{EI}{\rho S}}, \tag{3}$$

where l and r are the length and radius of the cantilever, respectively, $\rho \simeq 1.2$ g/cm^3 is the mass density of SU-8, and S is the cross sectional area of the cantilever. Using this expression one would find the resonant frequency of 204 kHz, which is typical to commercially available Si or Si_3N_4 cantilevers. The elastic properties of 3D PhC structures polymerized in SU-8 (Ref. 121) can also be used for elastic tuning of the photonic stopgap by via reversible deformation of the structure within the typical elasticity limit of up to 10% stress.[132] The effective Young's modulus of highly porous 3D structures fabricated by DLW can comprise just a fraction of that of solid SU-8.

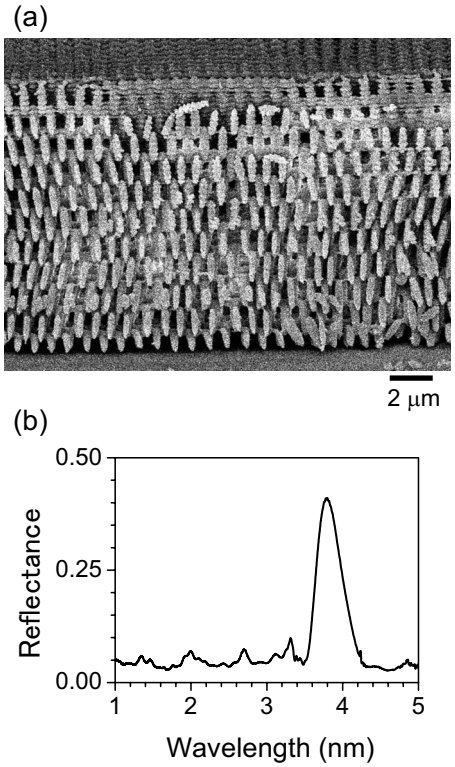

FIG. 8. (a) Side-view SEM image of a cleaved edge of a 3D structure recorded by five-beam interference via photopolymerization of SU-8 induced by non-linear absorption. (b) Measured optical reflectivity of the structure with a dominant reflectance peak due to PSG near 3.8 micrometers wavelength.

B. Holographic recording

The main advantage of holographic recording is its parallel nature, which can be contrasted with the sequential nature of DLW. This method can render 3D periodic structures via a single exposure event. It is also phase sensitive, which provides an opportunity to alter the periodic symmetry of the interference pattern by controlling the phases of the interfering beams or pulses.

Figure 8 illustrates the structural and optical properties of a structure recorded in SU-8 by the interference of five beams obtained from a single beam using a DOE. The beams were converged on a thin film of SU-8 spin coated on a cover-glass substrate. The conversion was obtained using an objective lens with NA=1.35. The high NA optics resulted in large overlap angles of the beams. This resulted in a structure whose lattice period is close to the smallest lattice period obtainable using a DOE for beam splitting. The structure consists of elongated elliptical voxels (volume elements) partially connected to each other in a pattern, which can be informally characterized by a body-centered tetragonal (bct) 3D symmetry. The bct unit cell can be derived from a canonical body-centered cubic (bct) unit cell by stretching it along the z-axis (vertical direction). Along this direction the structure has a period of 2.0 μm, and the voxels exhibit a faint ripplelike modulation with a period of approximately 270 nm due to the interference between the incident and back reflected pulses. Some structural disorder which is visible in the cleaved edge may be the result of sample cleavage rather than insufficient quality of fabrication. The optical re-

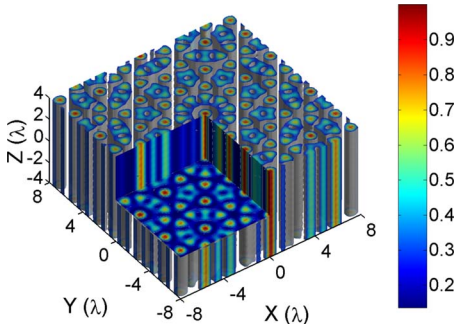

FIG. 9. (Color online) Theoretical five-beam interference pattern obtained from Eq. (1) at the overlap angle of 34° (an angle with the optical axis). The angular separation of all five beams around the optical axis was same 360°/5=72° with no central beam.

flection spectrum of the structure in Fig. 8(b) shows an intense reflective peak near the 3.8 μm wavelength due to a PSB.

Besides periodic structures, holographic recording can also be used to obtain quasiperiodic structures. Two-dimensional structures with five-, ten-, and 12-fold symmetries, Archimedean tilling, and Penrose lattices are attractive because they can provide functionality that is similar to that of periodic PhCs. In addition, they are expected to aid in omnidirectional light extraction from light-emitting diodes and in optical waveguiding.[133–135] The light interference patterns needed for quasicrystal recording can be conveniently generated using five or more beams obtained from a DOE beamsplitter. Figure 9 shows the interference patterns calculated from Eq. (1) for five beams with incidence angles distributed evenly around the axis of focusing (no central beam). The result of their interference is a 2D quasiperiodic pattern with fivefold symmetry. These and other patterns can be easily transferred to SU-8 or other photoresists.

To increase the resolution of holographic recording, the beam convergence angles must be increased using the prism setup shown schematically in Fig. 2. Laser pulses of about 100 fs temporal length have a spatial length of only about 30 μm. This length determines the maximum allowed optical path difference between the incident beams. Under these circumstances, timing between the pairs of participating pulses can be adjusted by maximizing the intensity of two-photon photoluminescence[136] emitted from a thin layer of dye $C_{40}H_{54}N_2O_2$ (Ref. 137) or a similar dye solution positioned at the focal plane. A five-beam interference pattern with angles of incidence of 70.53° was used for recording the pattern described in Fig. 3 above. Figure 10(a) shows an optical microscopy image of the photopolymerized SU-8 region after the development. The overall shape of this region is irregular, most likely due to substantial deviations of the intensity distribution of the beams from ideal Gaussian distributions. One can identify the outlines of two nearly vertical and one diagonal linear features, which originate from pairs of overlapping horizontally and diagonally aligned side beams. Coincidentally, the polymerized stripes have widths of approximately 25 μm, which corresponds to about half of the temporal overlap between the pulses, $c\tau_p/\sin(70.54°) \simeq 47$ μm. Under these circumstances, the intensity ratios be-

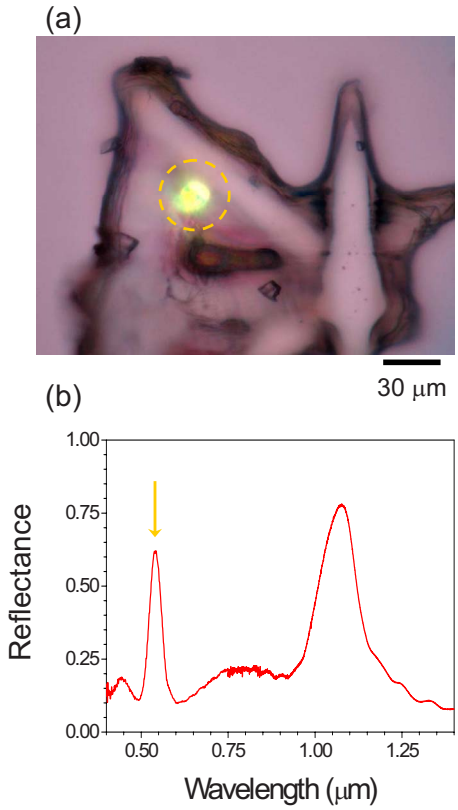

FIG. 10. (Color online) (a) Optical image of a photopolymerized SU-8 region after exposure to a five-beam interference pattern and development. The bright encircled region is a reflection resulting from illumination by a focused white-light source and has a dominant green color. (b) Optical reflection spectrum along the normal to the surface with two dominant reflection peaks due to PSGs. The arrow emphasizes the reflection centered at the 520 nm wavelength, which is most likely a second-order PSG responsible for the green color of the encircled area in the panel (a).

tween the interfering beams and the contrast of the interference pattern vary across the irradiated area. Careful examination of the sample has allowed identification of certain areas with appropriate beam intensity ratios and total exposure dose. For example, the area emphasized by the circle in Fig. 10(a) exhibits a specular reflection of bright green color. Its measured reflectivity spectrum exhibits an intense spectral peak near a wavelength of 520 nm [Fig. 10(b)], and another peak at a wavelength of 1.1 μm which is approximately twice as long. The first and second peaks most likely represent the second-order and fundamental PSB of the structure.[58] Observation of the second-order gap is evidence of good structural quality of the sample in the examined area. This is because higher-order stop gaps are sensitive to disorder and therefore do not occur in low quality structures. Figure 11 shows a SEM image of the structure (in this case, a different area located near the sample edge was selected for better visual assessment). Although the examined area is somewhat disordered, a lattice period of about 570 nm can be determined from the SEM image. Thus, although the contrast of the interference pattern and the dielectric volume filling fraction of the structure were far from optimal, these experiments provide a proof-of-principle demonstration for holographic fabrication of 3D structures using femtosecond pulses overlapped at high mutual angles.

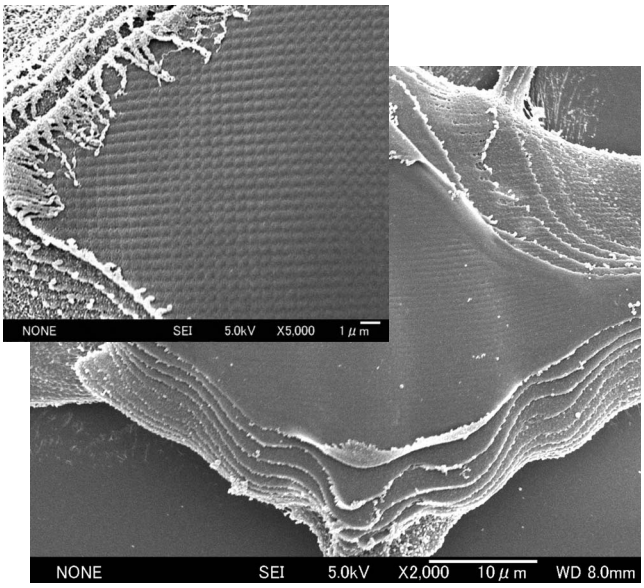

FIG. 11. SEM image of a structure fabricated by five-beam interference recording in SU-8. The average intensity ratio between the peripheral and the central beams was 1:3 (the optimal ratio is 1:16).

C. Postprocessing techniques

1. Postexposure retrieval of polymerized structures

The final step in processing the exposed samples involves their retrieval using developer or rinse solutions. 3D highly porous structures composed of features with submicrometric lateral size may be extremely sensitive to mechanical disturbances, which inevitably arise due to the surface tension and action of the capillary forces in the liquid developer or rinse filling pores of the structure. As a consequence, polymeric microstructures in resins and photoresists may become strongly deformed or totally destroyed during drying. These factors may be eliminated by using supercritical drying (SCD).[138,139] In supercritical liquids, surface tension becomes negligible and the capillary force vanishes. However, SCD requires a high pressure (1–10 MPa) and an elevated temperature (40–400 °C),[140] that depend on the solvent. For example, in order to use SCD for isopropanol (which is commonly used as a rinsing agent) removal from developed SU-8 networks, a temperature of over 235.2 °C, and a pressure of over 4.8 MPa are required.[140] These conditions are too destructive for SU-8, and surface tension and capillary forces must be suppressed using other means, which are briefly described below.

Dewetting of the surfaces of the polymeric features results in the formation of patterns of droplets when liquid evaporates. This phenomenon is very general, and, for example, governs the Stranski–Krastanov mechanism of thin film breakup into quantum dots.[141,142] The surface tension generates forces between the materials that are in contact (solid, liquid, and air) that control dewetting. Dewetting is difficult to control during the fabrication of ordered patterns[143] (in some cases it is possible to fabricate structures with intentionally distorted shapes, which are later compensated by distortions due to capillary shrinkage,[144,145] but such structures may have poor long-term mechanical stability). The distortion of photopolymerized structures during drying can be understood in terms of evaporation coupled with energy minimization during the capillary drainage.[146] Evaporation decreases the content of liquid infiltrating the porous structure, and the capillary forces pull solid polymeric features, causing them to bend and deform. This process may proceed until the structure fully collapses. The collapse of the pattern can be prevented by controlling the evaporation rate of the liquid or by reducing the capillary forces. For example, the inherent hydrophobicity of SU-8 polymers may help facilitate reduction of the capillary forces if water is used as a rinse agent instead of isopropanol.[147] Since it is known that the mechanical properties of photopolymerized structures depend on the degree of cross-linking,[119,132] additional UV exposure of the structure may be applied prior to its removal from the liquid (water is transparent in the UV spectral range).

2. Infiltration by other materials

Optical fabrication is performed mostly on materials that have moderate refractive indices. Most of the inorganic and organic glasses, and polymers, including photocurable resins and photoresists have refractive indices in the range of $n \approx 1.45-1.7$. Hence, if porous structures are obtained from these initial materials using laser microfabrication, their refractive index contrast is defined by the index values of the host material and air ($n=1$). On the other hand, theoretical analysis of PhCs and their photonic band dispersion properties has indicated that an index contrast of at least $\Delta n \simeq 2$ is required in order to open PBGs in 3D structures. Hence, fabricated polymeric PhCs fabricated in polymers and glass can only demonstrate PSBs or bands of optical attenuation only along certain directions. Of course, various high refractive index materials are available. For example, semiconductors such as Si and GaAs behave as high refractive index $n \approx 3.5$ dielectrics at photon energies below the fundamental absorption edge. Titania (TiO_2) has a refractive index of $n=2.49$ (2.9) for anatase (rutile) phases, zirconia has (ZrO_2) $n \approx 2.2$, diamond has $n \approx 2.45$, and various chalcogenide glasses have $n > 2.5$. However, refractive index mismatches between the focusing optics made of silica-based glass ($n \approx 1.47$) and the fabricated medium create strong optical aberrations, which begin to limit the resolution of the structure. This is the main reason that the best-quality structures are obtained in low-index photosensitive resins and polymers. To improve the index contrast, these structures are used as templates, into which high-index materials can be infiltrated using a variety of techniques. Subsequently, the original template can be removed by thermal or chemical treatment, thereby enhancing the index contrast. Single- and double-infiltration methods were first applied to enhance low-index synthetic opals. These techniques involved high-temperature chemical vapor deposition (CVD) and were therefore unsuitable for polymeric structures whose thermal stability was compromised at temperatures above 200–300 °C. Later, the infiltration process was adapted for polymeric structures by introducing an intermediate step in which a heat-resistant sacrificial material (e.g., silica) was infiltrated using a low-temperature sol-gel process. After that, the original template was removed thermally, and a high refractive index semicon-

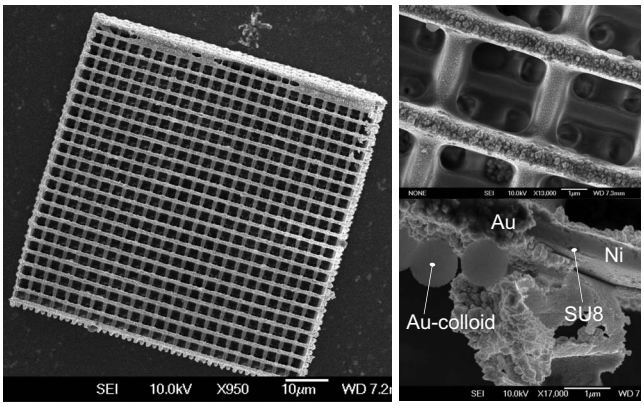

FIG. 12. SEM images of a 3D SU-8 woodpile structure coated by Ni and Au using electroless plating technique (courtesy of Dr. R. Tarozaitė).

ductor (e.g., Si) was infiltrated into the voids by CVD, creating a high-index replica of the initial polymeric structure. Silicon PhC structures with woodpile and spiral topologies[148] have been successfully fabricated using this approach. The templates were initially prepared from SU-8 by DLW, and the final structures were shown to faithfully replicate the initial templates.

The above processing steps enhance index contrast but do not modify the dielectric nature of the templates. However, bearing in mind recent developments in the fields of plasmonics and metamaterials,[4,6,28,149–151] the possibility of transforming a dielectric PhC structures into a metallic (or metalodielectric) structure is quite intriguing.

Photopolymerized structures and the subsequent metallized 3D structures have large surface area to volume ratio and are expected to find an increasing number of applications as fuel cells, supercapacitors, superadhesives, scaffolds for biomolecules, and tissue engineering for implants,[152] or in space applications where mass(strength)-to-volume ratio is critical. Moreover, such polymer patterns can be coated by noble, catalytic, or magnetic metals using a simple chemical electroless deposition by dipcoating. Recently, electroless coating of SU-8 woodpile patterns by nickel, which has the relative magnetic permeability only twice lower than that of magnetic iron, was demonstrated.[153] The reflection spectrum of such metalodielectric PhC structures can be engineered for IR applications where they act as band-edge filters.[153] The conductivity of 3D polymeric structures coated by metals can be further exploited for electroless or electrochemical plating by other metals. Once surfaces acquire electric conductivity, they can be used in supercapacitor or electrophoretic applications. The 3D structured templates coated by magnetic materials show large out-of-plane magnetization perpendicular to the coated film. This effect is due to pinning of the domain boundaries by the nano-/microstructure which could be extremely useful for high-density memory applications.[154]

To illustrate metallization of SU-8 woodpile templates, Fig. 12 shows a SEM image of a structure which was first infiltrated by a nickel film via electroless dip coating.[153] A second coating of gold was later applied by immersion into a gold plating solution.

V. CONCLUSIONS

We have presented a brief overview of materials that have potential uses for photonic, fluidic, mechanical, and other applications. The materials we discussed were obtained via 3D optical structuring of initially homogeneous materials using femtosecond laser pulses. We have discussed in some depth how laser-fabricated 3D structures offer an easy route for creating functional PhCs via infiltration by high-index materials. The field of femtosecond laser microfabrication is still far from maturity. Its potential to become a leading technique for microfabrication is high. This technique is expected to deliver micro- and nanoscale devices in a cost-effective and efficient manner. One particularly interesting area of application, which was omitted from this review, is the use of femtosecond laser microfabrication for the creation of biocompatible materials, such as scaffolds suitable for culturing cells and tissues.

The full range of possible applications for optically engineered materials and systems goes beyond the scope of this paper. This area of research is likely to undergo a rapid development in the future.

ACKNOWLEDGMENTS

The authors acknowledge financial support provided by Grant-in-Aid Nos. 19360322 and 19049001 for Scientific Research on the Priority Area "Strong Photon-Molecule Coupling Fields for Chemical Reactions" (No. 470) from the Ministry of Education, Science, Sports, and Culture of Japan. The authors are grateful to Professor S. John for discussions on 3D PhC design, K. Kannari for technical assistance in sample preparation, to Professor S. Tanaka for help with TEM measurements, Dr. M. Farsari for discussions on sol-gel resists, and Dr. Z. Bomzon for critical remarks on the manuscript.

[1] M. Tennant, *Nanotechnology* (AIP, New York, 1999).
[2] S. John, Phys. Rev. Lett. **58**, 2486 (1987).
[3] E. Yablonovitch, Phys. Rev. Lett. **58**, 2059 (1987).
[4] G. Dolling, C. Enkrich, M. Wegener, C. M. Soukoulis, and S. Linden, Opt. Lett. **31**, 1800 (2006).
[5] J. B. Pendry, L. Martn-Moreno, and F. J. Garcia-Vidal, Science **305**, 847 (2004).
[6] V. M. Shalaev, W. Cai, U. K. Chettiar, H.-K. Yuan, A. K. Sarychev, V. P. Drachev, and A. V. Kildishev, Opt. Lett. **30**, 3356 (2005).
[7] M. Qi, E. Lidorikis, P. Rakich, S. Johnson, J. Joannopoulos, E. Ippen, and H. Smith, Nature (London) **429**, 538 (2004).
[8] V. S. Amaratunga, H. T. Hattori, M. Premaratne, H. H. Tan, and C. Jagadish, J. Opt. Soc. Am. B **25**, 1532 (2008).
[9] I. Tarhan and G. H. Watson, Phys. Rev. Lett. **76**, 315 (1996).
[10] A. Blanco, E. Chomski, S. Grabtchak, M. Ibisate, S. John, S. Leonard, C. Lopez, F. Meseguer, H. Miguez, J. Mondia, G. Ozin, O. Toader, and H. van Driel, Nature (London) **405**, 437 (2000).
[11] V. Mizeikis, K. K. Seet, S. Juodkazis, and H. Misawa, Opt. Lett. **29**, 2061 (2004).
[12] M. Deubel, G. von Freymann, M. Wegener, S. Pereira, K. Busch, and C. Soukoulis, Nature Mater. **3**, 444 (2004).
[13] M. Deubel, M. Wegener, and A. Kaso, Appl. Phys. Lett. **85**, 1895 (2004).
[14] H. Sun, Y. Xu, S. Juodkazis, K. Sun, M. Watanabe, S. Matsuo, H. Misawa, and J. Nishii, Opt. Lett. **26**, 325 (2001).
[15] H. Sun, V. Mizeikis, S. Juodkazis, J.-Y. Ye, S. Matsuo, and H. Misawa, Appl. Phys. Lett. **79**, 1 (2001).
[16] F. E. Livingston and H. Helvajian, MRS Bull. **32**, 40 (2007).
[17] K. K. Seet, V. Mizeikis, S. Matsuo, S. Juodkazis, and H. Misawa, Adv. Mater. (Weinheim, Ger.) **17**, 541 (2005).

[18]K. K. Seet, V. Mizeikis, S. Juodkazis, and H. Misawa, Appl. Phys. Lett. **88**, 221101 (2006).
[19]T. Kondo, S. Matsuo, S. Juodkazis, and H. Misawa, Appl. Phys. Lett. **79**, 725 (2001).
[20]T. Kondo, S. Matsuo, S. Juodkazis, V. Mizeikis, and H. Misawa, Appl. Phys. Lett. **82**, 2758 (2003).
[21]D. Melville and R. Blaikie, Opt. Express **13**, 2127 (2005).
[22]S. Y. Chou, P. R. Krauss, and P. J. Renstrom, Science **272**, 85 (1996).
[23]N. Tetreault, G. von Freymann, M. Deubel, M. Hermatschweiler, F. Pérez-Willard, S. John, M. Wegener, and G. A. Ozin, Adv. Mater. (Weinheim, Ger.) **18**, 457 (2006).
[24]K. Busch, G. von Freymann, S. Linden, S. F. Mingaleev, and L. T. M. Wegener, Phys. Rep. **444**, 101 (2007).
[25]J. Serbin and M. Gu, Adv. Mater. (Weinheim, Ger.) **18**, 221 (2006).
[26]J. Serbin, A. Egbert, A. Ostendorf, B. N. Chichkov, R. H. G. Domann, J. Schulz, C. Cronauer, L. Frohlich, and M. Popall, Opt. Lett. **28**, 301 (2003).
[27]M. Thiel, M. Decker, M. Deubel, M. Wegener, S. Linden, and G. Freymann, Adv. Mater. (Weinheim, Ger.) **19**, 207 (2007).
[28]M. S. Rill, C. Plet, M. Thiel, I. Staude, G. von Freymann, and S. Linden, and M. Wegener, Nature Mater. **7**, 543 (2008).
[29]K. Sakoda, *Optical Properties of Photonic Crystals*, Springer Series in Optical Sciences, Vol. 80 (Springer, New York, 2001).
[30]J. D. Joannopoulos, S. G. Johnson, J. N. Winn, and R. D. Meade, *Photonic Crystals: Molding the Flow of Light* (Princeton University Press, Princeton, 2008).
[31]A. Argyros, S. Manos, M. Large, D. McKenzie, G. Cox, and D. Dwarte, Micron **33**, 483 (2002).
[32]A. Saito, Y. Miyamura, M. Nakajima, Y. Ishikawa, K. Sogo, Y. Kuwahara, and Y. Hirai, J. Vac. Sci. Technol. A **24**, 3248 (2006).
[33]H. Masuda and K. Fukuda, Science **268**, 1466 (1995).
[34]M. H. Kluhr, A. Sauermann, C. A. Elsner, K. H. Thein, and S. Dertinger, Adv. Mater. (Weinheim, Ger.) **18**, 3135 (2006).
[35]I. Mikulskas, S. Juodkazis, R. Tomašiūnas, and J. G. Dumas, Adv. Mater. (Weinheim, Ger.) **13**, 1574 (2001).
[36]V. Mizeikis, I. Mikulskas, R. Tomašiūnas, S. J. S. Matsuo, and H. Misawa, Jpn. J. Appl. Phys., Part 1 **43**, 3643 (2004).
[37]V. Lehmann, Appl. Surf. Sci. **106**, 402 (1996).
[38]J. Jakubowicz, Superlattices Microstruct. **41**, 205 (2007).
[39]V. Lehman and H. Föll, J. Electrochem. Soc. **137**, 653 (1990).
[40]V. Lehman, J. Electrochem. Soc. **140**, 2836 (1993).
[41]V. Lehman and U. Grüning, Thin Solid Films **297**, 13 (1997).
[42]J. Wang, H. Niino, and A. Yabe, Appl. Phys. A: Mater. Sci. Process. **68**, 111 (1999).
[43]G. Kopitkovas, T. Lippert, C. David, A. Wokaun, and J. Gobrecht, Thin Solid Films **453**, 31 (2004).
[44]R. Bohme, J. Zajadacz, K. Zimmer, and B. Rauschenbach, Appl. Phys. A **80**, 433 (2005).
[45]C. Monat, P. Domachuk, and B. J. Eggleton, Nat. Photonics **1**, 106 (2007).
[46]D. Psaltis, S. R. Quake, and C. Yang, Nature (London) **442**, 381 (2006).
[47]H. Misawa and S. Juodkazis, Prog. Polym. Sci. **24**, 665 (1999).
[48]T.-H. Lin, Y.-J. Chen, C.-H. Wu, and Y.-G. Fuh, Appl. Phys. Lett. **86**, 161120 (2005).
[49]V. A. Mallia and N. Tamaoki, Chem. Soc. Rev. **33**, 76 (2004).
[50]K. Yoshino, Y. Shimoda, Y. Kawagishi, K. Nakayama, and M. Ozaki, Appl. Phys. Lett. **75**, 932 (1999).
[51]A. F. Muñoz, P. Palffy-Muhoray, and B. Taheri, Opt. Lett. **26**, 804 (2001).
[52]H. Finkelmann, S. T. Kim, A. Munoz, P. Palffy-Muhoray, and B. Taheri, Adv. Mater. (Weinheim, Ger.) **13**, 1069 (2001).
[53]T. Matsui, R. Ozaki, K. Funamoto, M. Ozaki, and K. Yoshino, Appl. Phys. Lett. **81**, 3741 (2002).
[54]K. K. Seet, V. Mizeikis, S. Juodkazis, and H. Misawa, J. Non-Cryst. Solids **352**, 2390 (2006).
[55]O. Toader and S. John, Science **292**, 1133 (2001).
[56]A. Ledermann, L. Cademartiri, M. Hermatschweiler, C. Toninelli, G. Ozin, D. Wiersma, M. Wegener, and G. von Freymann, Nature Mater. **5**, 942 (2006).
[57]V. Mizeikis, H.-B. Sun, A. Marcinkevicius, J. Nishii, S. J. S. Matsuo, and H. Misawa, J. Photochem. Photobiol., A **145**, 41 (2001).
[58]M. Straub, M. Ventura, and M. Gu, Phys. Rev. Lett. **91**, 043901 (2003).
[59]M. J. Ventura, M. Straub, and M. Gu, Appl. Phys. Lett. **82**, 1649 (2003).
[60]O. Efimov, S. Juodkazis, and H. Misawa, Phys. Rev. A **69**, 042903 (2004).
[61]E. Vanagas, J. Kawai, D. Tuzilin, I. Kudryashov, A. Mizuyama, K. G. Nakamura, K.-I. Kondo, S.-Y. Koshihara, M. Takesada, K. Matsuda, S. Juodkazis, V. Jarutis, S. Matsuo, and H. Misawa, J. Microlithogr., Microfabr., Microsyst. **3**, 358 (2004).
[62]E. Vanagas, I. Kudryashov, D. Tuzhilin, S. Juodkazis, S. Matsuo, and H. Misawa, Appl. Phys. Lett. **82**, 2901 (2003).
[63]A. Marcinkevicius, S. Juodkazis, S. Matsuo, V. Mizeikis, and H. Misawa, Jpn. J. Appl. Phys., Part 2 **40**, L1197 (2001).
[64]E. Gaižauskas, E. Vanagas, V. Jarutis, S. Juodkazis, V. Mizeikis, and H. Misawa, Opt. Lett. **31**, 80 (2006).
[65]S. Matsui, T. Kaito, J.-I. Fujita, M. Komuro, K. Kanda, and Y. Haruyama, J. Vac. Sci. Technol. B **18**, 3181 (2000).
[66]B. Stuart, M. Feit, A. Rubenchik, S. Herman, B. Shore, and M. Perry, Phys. Rev. B **53**, 1749 (1996).
[67]T. Hashimoto, S. Juodkazis, and H. Misawa, New J. Phys. **9**, 253 (2007).
[68]E. E. Gamaly, S. Juodkazis, K. Nishimura, H. Misawa, B. L.-D. L. Hallo, P. Nicolai, and V. Tikhonchuk, Phys. Rev. B **73**, 214101 (2006).
[69]K. Yamasaki, S. Juodkazis, S. Matsuo, and H. Misawa, Appl. Phys. A: Mater. Sci. Process. **77**, 371 (2003).
[70]G. Zhou, M. Ventura, M. Vanner, and M. Gu, Appl. Phys. Lett. **86**, 011108 (2005).
[71]K. Miura, J. Qiu, H. Inouye, T. Mitsuyu, and K. Hirao, Appl. Phys. Lett. **71**, 3329 (1997).
[72]S. Juodkazis, Y. Nishi, and H. Misawa, Phys. Stat. Sol. (RRL) 2 **1–3**, 275 (2008).
[73]H. Sun, S. Matsuo, and H. Misawa, Appl. Phys. Lett. **74**, 786 (1999).
[74]S. Kawata, H.-B. Sun, T. Tanaka, and K. Takada, Nature (London) **412**, 697 (2001).
[75]G. Witzgall, R. Vrijen, E. Yablonovitch, V. Doan, and B. Schwartz, Opt. Lett. **23**, 1745 (1998).
[76]MicroChem Corp. http://www.microchem.com/products/su_eight.htm.
[77]T. Y. M. Chan and S. John, Phys. Rev. A **78**, 033812 (2008).
[78]T. Chan, O. Toader, and S. John, Phys. Rev. E **71**, 046605 (2005).
[79]O. Toader, T. Chan, and S. John, Phys. Rev. Lett. **92**, 043905 (2004).
[80]T. Kondo, S. Juodkazis, V. Mizeikis, S. Matsuo, and H. Misawa, New J. Phys. **8**, 250 (2006).
[81]T. Kondo, S. Juodkazis, V. Mizeikis, H. Misawa, and S. Matsuo, Opt. Express **14**, 7943 (2006).
[82]A. A. Maznev, T. F. Crimmins, and K. A. Nelson, Opt. Lett. **23**, 1378 (1998).
[83]T. Kondo, K. Yamasaki, S. Juodkazis, S. Matsuo, and V. M. H. Misawa, Thin Solid Films **453–454**, 550 (2004).
[84]S. Juodkazis, T. Kondo, V. Mizeikis, S. Matsuo, H. Murata, and H. Misawa, Proc. SPIE **4977**, 94 (2003).
[85]Y. V. Miklyaev, D. C. Meisel, A. Blanco, G. von Freymann, K. Busch, W. Koch, C. Enkrich, M. Deubel, and M. Wegener, Appl. Phys. Lett. **82**, 1284 (2003).
[86]O. Toader, T. Y. M. Chan, and S. John, Appl. Phys. Lett. **89**, 101117 (2006).
[87]T. Y. M. Chan, O. Toader, and S. John, Phys. Rev. E **73**, 046610 (2006).
[88]D. Chanda, L. Abolghasemi, M. Haque, M. Ng, and P. Herman, Opt. Express **16**, 15402 (2008).
[89]D. B. Shao and S. C. Chen, Nano Lett. **6**, 2279 (2006).
[90]K. M. Davis, K. Miura, N. Sugimoto, and K. Hirao, Opt. Lett. **21**, 1729 (1996).
[91]V. Mizeikis, S. Juodkazis, A. Marcinkevicius, S. Matsuo, and H. Misawa, J. Photochem. Photobiol. C **2**, 35 (2001).
[92]S. Juodkazis, S. Matsuo, H. Misawa, V. Mizeikis, A. M. H. B. Sun, Y. Tokuda, M. Takahashi, T. Yoko, and J. Nishii, Appl. Surf. Sci. **197–198**, 705 (2002).
[93]S. Juodkazis, K. Yamasaki, V. Mizeikis, S. Matsuo, and H. Misawa, Appl. Phys. A: Mater. Sci. Process. **79**, 1549 (2004).
[94]A. Marcinkevicius, S. Juodkazis, M. Watanabe, M. Miwa, S. M. H. Misawa, and J. Nishii, Opt. Lett. **26**, 277 (2001).
[95]M. Watanabe, H.-B. Sun, S. Juodkazis, T. Takahashi, S. M. Y. Suzuki, J. Nishii, and H. Misawa, Jpn. J. Appl. Phys., Part 2 **37**, L1527 (1998).
[96]S. Juodkazis, A. V. Rode, E. G. Gamaly, S. Matsuo, and H. Misawa, Appl. Phys. B: Lasers Opt. **77**, 361 (2003).
[97]S. Juodkazis, M. Sudzius, V. Mizeikis, H. Misawa, E. G. G. Y. Liu, O. A. Louchev, and K. Kitamura, Appl. Phys. Lett. **89**, 062903 (2006).
[98]M. Watanabe, S. Juodkazis, H.-B. Sun, S. Matsuo, H. Misawa, M. Miwa, and R. Kaneko, Appl. Phys. Lett. **74**, 3957 (1999).
[99]M. Watanabe, S. Juodkazis, H.-B. Sun, S. Matsuo, and H. Misawa, Phys. Rev. B **60**, 9959 (1999).
[100]K. Yamasaki, S. Juodkazis, M. Watanabe, H.-B. Sun, and S. M. H. Misawa, Appl. Phys. Lett. **76**, 1000 (2000).

[101] F. Formanek, N. Takeyasu, T. Tanaka, K. Chiyoda, and A. I. S. Kawata, Appl. Phys. Lett. **88**, 083110 (2006).
[102] S. Matsuo, S. Juodkazis, and H. Misawa, Appl. Phys. A: Mater. Sci. Process. **80**, 683 (2004).
[103] C. Mauclair, A. Mermillod-Blondin, N. Huot, E. Audouard, and R. Stoian, Opt. Express **16**, 5481 (2008).
[104] H. Takahashi, S. Hasegawa, A. Takita, and Y. Hayasaki, Opt. Express **16**, 16592 (2008).
[105] T. Hashimoto, S. Juodkazis, and H. Misawa, Appl. Phys. A: Mater. Sci. Process. **83**, 337 (2006).
[106] S. Juodkazis, H. Misawa, T. Hashimoto, E. Gamaly, and B. Luther-Davies, Appl. Phys. Lett. **88**, 201909 (2006).
[107] S. Juodkazis, K. Nishimura, S. Tanaka, H. Misawa, E. E. G. B. Luther-Davies, L. Hallo, P. Nicolai, and V. Tikhonchuk, Phys. Rev. Lett. **96**, 166101 (2006).
[108] S. Juodkazis, K. Nishimura, H. Misawa, T. Ebisui, R. Waki, S. Matsuo, and T. Okada, Adv. Mater. (Weinheim, Ger.) **18**, 1361 (2006).
[109] S. Juodkazis, K. Nishimura, and H. Misawa, Chin. Opt. Lett. **5**, S198 (2007).
[110] M. Mazilu, S. Juodkazis, T. Ebisui, and H. Misawa, Appl. Phys. A: Mater. Sci. Process. **86**, 197 (2007).
[111] A. Marcinkevicius, V. Mizeikis, S. Juodkazis, S. Matsuo, and H. Misawa, Appl. Phys. A: Mater. Sci. Process. **76**, 257 (2003).
[112] N. Huot, R. Stoian, A. Mermillod-Blondin, C. Mauclair, and E. Audouard, Opt. Express **15**, 12395 (2007).
[113] E. G. Gamaly, S. Juodkazis, V. Mizeikis, H. Misawa, A. V. R. W. Z. Krolikowski, and K. Kitamura, Curr. Appl. Phys. **8**, 416 (2008).
[114] S. Juodkazis, T. Kondo, H. Misawa, A. Rode, M. Samoc, and B. Luther-Davies, Opt. Express **14**, 7751 (2006).
[115] Z. Sacks, G. Mourou, and R. Danielius, Opt. Lett. **26**, 462 (2001).
[116] R. Wolleschensky, T. Feurer, R. Sauerbrey, and U. Simon, Appl. Phys. B: Lasers Opt. **67**, 87 (1998).
[117] K. Yamasaki, S. Juodkazis, T. Lippert, M. Watanabe, and S. M. H. Misawa, Appl. Phys. A: Mater. Sci. Process. **76**, 325 (2003).
[118] S. Juodkazis, K. Yamasaki, S. Matsuo, and H. Misawa, Appl. Phys. Lett. **84**, 514 (2004).
[119] S. Juodkazis, V. Mizeikis, S. Matsuo, K. Ueno, and H. Misawa, Bull. Chem. Soc. Jpn. **81**, 411 (2008).
[120] V. R. Bhardwaj, E. Simova, P. P. Rajeev, C. Hnatovsky, R. D. Rayner, and P. B. Corkum, Phys. Rev. Lett. **96**, 057404 (2006).
[121] S. Juodkazis, V. Mizeikis, and H. Misawa, Adv. Polym. Sci. **213**, 157 (2008).
[122] S. Juodkazis, K. Nishimura, H. Okuno, Y. Tabuchi, S. M. S. Tanaka, and H. Misawa, Proc. SPIE **6732**, 67320B (2007).
[123] K. J. Schafer, J. M. Hales, M. Balu, K. D. Belfield, E. W. Van Stryland, and D. J. Hagan, J. Photochem. Photobiol., A **162**, 497 (2004).
[124] K. K. Seet, S. Juodkazis, V. Jarutis, and H. Misawa, Appl. Phys. Lett. **89**, 024106 (2006).
[125] R. Houbertz, L. Frählich, M. Popall, U. Streppel, P. Dannberg, A. Bräuer, J. Serbin, and B. Chichkov, Adv. Eng. Mater. **5**, 551 (2003).
[126] A. Ovsiannikov, A. Gaidukeviciute, B. Chichkov, M. Oubaha, B. MacCraith, I. Sakellari, A. Giakoumaki, D. Gray, M. Vamvakaki, M. Farsari, and C. Fotakis, Laser Chem. **2008**, 493059 (2008).
[127] A. Ovsianikov, S. Z. Xiao, M. Farsari, M. Vamvakaki, C. Fotakis, and B. N. Chichkov, Opt. Express **17**, 2143 (2009).
[128] K. K. Seet, V. Mizeikis, S. Juodkazis, and H. Misawa, Appl. Phys. A: Mater. Sci. Process. **82**, 683 (2006).
[129] M. Thiel, G. von Freymann, and M. Wegener, Opt. Lett. **32**, 2547 (2007).
[130] K. M. Ho, C. T. Chan, C. M. Soukoulis, R. Biswas, and M. Sigalas, Solid State Commun. **89**, 413 (1994).
[131] R. M. Digilov, Eur. J. Phys. **29**, 589 (2008).
[132] S. Juodkazis, V. Mizeikis, K. K. Seet, H. Misawa, and U. G. K. Wegst, Appl. Phys. Lett. **91**, 241904 (2007).
[133] M. E. Zoorob, M. D. B. Charlton, G. J. Parker, J. J. Baumberg, and M. C. Netti, Nature (London) **404**, 740 (2000).
[134] A. David, T. Fujii, E. Matioli, R. Sharma, S. Nakamura, S. P. DenBaars, and C. Weisbuch, Appl. Phys. Lett. **88**, 073510 (2006).
[135] R. C. Gauthier, Opt. Commun. **269**, 395 (2007).
[136] N. Murazawa, S. Juodkazis, H. Misawa, and K. Kamada, Mol. Cryst. Liq. Cryst. **489**, 310 (2008).
[137] M. Rumi, J. Ehrlich, A. Heikal, J. Perry, S. Barlow, Z. Hu, D. McCord-Maughon, T. C. Parker, H. Rockel, S. Thayumanavan, S. R. Marder, D. Beljonne, and J.-L. Bredas, J. Am. Chem. Soc. **122**, 9500 (2000).
[138] M. A. McHugh and V. J. Krukonis, *Supercritical Fluid Extraction*, 2nd ed. (Butterworth-Heinemann, Boston, 1994).
[139] C. A. Eckert, B. L. Knutson, and P. G. Debendetti, Nature (London) **383**, 313 (1996).
[140] *Organic Solvents. Physical Properties and Methods of Purification*, 4th ed., edited by A. Weissberger (Wiley, New York, 1986).
[141] T. Tawara, S. Tanaka, H. Kumano, and I. Suemune, Appl. Phys. Lett. **75**, 235 (1999).
[142] I. Suemune, T. Tawara, T. Saitoh, and K. Uesugi, Appl. Phys. Lett. **71**, 3886 (1997).
[143] Y. Hashimoto and O. Karthaus, J. Colloid Interface Sci. **311**, 289 (2007).
[144] H.-B. Sun, T. Suwa, K. Takada, R. P. Zaccaria, M. S. Kim, K. S. Lee, and S. Kawata, Appl. Phys. Lett. **85**, 3708 (2004).
[145] D. C. Meisel, M. Diem, M. Deubel, F. Perez-Willard, S. L. D. Gerthsen, K. Busch, and M. Wegener, Adv. Mater. (Weinheim, Ger.) **18**, 2964 (2006).
[146] S. Juodkazis, V. Mizeikis, T. Kondo, K. Kannari, K. K. Seet, and H. Misawa, Proc. SPIE **6883**, 68830I (2008).
[147] T. Kondo, S. Juodkazis, and H. Misawa, Appl. Phys. A: Mater. Sci. Process. **81**, 1583 (2005).
[148] K. K. Seet, V. Mizeikis, K. Kannari, S. Juodkazis, H. M. N. Tetreault, and S. John, IEEE J. Sel. Top. Quantum Electron. **14**, 1064 (2008).
[149] G. Dolling, C. Enkrich, M. Wegener, C. M. Soukoulis, and S. Linden, Science **312**, 892 (2006).
[150] J. B. Pendry, Science **306**, 1353 (2004).
[151] M. C. Wiltshire, J. B. Pendry, I. R. Young, D. J. Larkman, D. J. Gilderdale, and J. V. Hajnal, Science **291**, 849 (2001).
[152] J. Lee, M. J. Cuddihy, and N. A. Kotov, Tissue Eng. **14**, 61 (2008).
[153] V. Mizeikis, S. Juodkazis, R. Tarozaitė, J. J. K. Juodkazis, and H. Misawa, Opt. Express **15**, 8454 (2007).
[154] R. P. Cowburn, A. O. Adeyeye, and J. A. C. Bland, Appl. Phys. Lett. **70**, 2309 (1997).